Limits on Charge Carrier Mobility in Suspended Graphene due to Flexural Phonons

Eduardo V. Castro,[1] H. Ochoa,[1] M. I. Katsnelson,[2] R. V. Gorbachev,[3] D. C. Elias,[3] K. S. Novoselov,[3] A. K. Geim,[3] and F. Guinea[1]

[1]*Instituto de Ciencia de Materiales de Madrid (CSIC), Sor Juana Inés de la Cruz 3, E-28049 Madrid, Spain*
[2]*Radboud University Nijmegen, Institute for Molecules and Materials, NL-6525 AJ Nijmegen, The Netherlands*
[3]*School of Physics & Astronomy and Manchester Centre for Mesoscience & Nanotechnology, University of Manchester, Manchester M13 9PL, United Kingdom*

(Received 21 August 2010; published 22 December 2010)

The temperature dependence of the mobility in suspended graphene samples is investigated. In clean samples, flexural phonons become the leading scattering mechanism at temperature $T \gtrsim 10$ K, and the resistivity increases quadratically with T. Flexural phonons limit the intrinsic mobility down to a few $m^2/V\,s$ at room T. Their effect can be eliminated by applying strain or placing graphene on a substrate.

DOI: 10.1103/PhysRevLett.105.266601 PACS numbers: 72.80.Vp, 63.22.Rc, 72.10.Di

Introduction.—Graphene continues to attract enormous interest due to both its exotic electronic properties [1] and realistic prospects of various applications [2]. It has been found that the intrinsic mobility μ of charge carriers in graphene can exceed 20 $m^2/V\,s$ at room temperature (T) [3,4], which is the absolute record. So far, such high values have not been achieved experimentally, because extrinsic scatterers limit μ. The highest μ was reported in suspended devices [5,6] and could reach ~ 12 $m^2/V\,s$ at 240 K [7]. This, however, disagrees with the data of Ref. [5], where similar samples exhibited room-T μ close to ~ 1 $m^2/V\,s$, the value that is routinely achievable for graphene on a substrate.

In this Letter, we show that flexural phonons (FP) are an important scattering mechanism in suspended graphene and the likely origin of the above disagreement, and their contribution should be suppressed to allow ultrahigh μ. Generally, electron-phonon scattering in graphene is expected to be weak due to very high phonon frequencies [8]. However, in suspended thin membranes, out of plane vibrations lead to a new class of low energy phonons, the flexural branch [9,10]. In an ideal flat suspended membrane symmetry arguments show that electrons can only be scattered by two FP simultaneously [3,11]. As a result the resistivity due to FP rises rapidly as T^2 at high T, where it can be described as elastic scattering by thermally excited intrinsic ripples [12].

We analyze here the contribution of FP to the resistivity, and present experimental results which strongly support the suggestion that FP are a major source of electron scattering in suspended graphene. This intrinsic limitation to the achievable conductivity of graphene at room T can be relaxed by applying tension, which modifies both the phonons and their coupling to charge carriers.

Model.—Graphene is a two dimensional membrane, whose elastic properties are well described by the free energy [9,10]:

$$\mathcal{F} \equiv \frac{1}{2}\kappa \int dxdy(\nabla^2 h)^2 + \frac{1}{2}\int dxdy(\lambda u_{ii}^2 + 2\mu u_{ij}^2), \quad (1)$$

where κ is the bending rigidity, λ and μ are Lamé coefficients, h is the displacement in the out of plane direction, and $u_{ij} = 1/2[\partial_i u_j + \partial_j u_i + (\partial_i h)(\partial_j h)]$ is the strain tensor. Summation over indices in Eq. (1) is implied. Typical parameters for graphene [13–15] are $\kappa \approx 1$ eV, and $\mu \approx 3\lambda \approx 9$ eV Å^{-2}. The density is $\rho = 7.6 \times 10^{-7}$ Kg/m^2. The velocities of the longitudinal and transverse phonons obtained from Eq. (1) are $v_L = \sqrt{\frac{\lambda+2\mu}{\rho}} \approx 2.1 \times 10^4$ m/s and $v_T = \sqrt{\frac{\mu}{\rho}} \approx 1.4 \times 10^4$ m/s. The FP show the dispersion

$$\omega_{\vec{q}}^F = \alpha |\vec{q}|^2 \quad (2)$$

with $\alpha = \sqrt{\frac{\kappa}{\rho}} \approx 4.6 \times 10^{-7}$ m^2/s.

Suspended graphene can be under tension, either due to the electrostatic force arising from the gate, or as a result of microfabrication. Let us assume that there are slowly varying in-plane stresses, $u_{ij}(\vec{r})$, which change little on the scale of the Fermi wavelength, k_F^{-1}, which is the relevant length for the calculation of the carrier resistivity. Then, the dispersion in Eq. (2) is changed into

$$\omega_{\vec{q}}^F(\vec{r}) = |\vec{q}|\sqrt{\frac{\kappa}{\rho}|\vec{q}|^2 + \frac{\lambda}{\rho}u_{ii}(\vec{r}) + \frac{2\mu}{\rho}u_{ij}(\vec{r})\frac{q_i q_j}{|\vec{q}|^2}}. \quad (3)$$

The dispersion becomes anisotropic. For small wave vectors, the dispersion is linear, with a velocity which scales as $\sqrt{\bar{u}}$, where $\bar{u}$ is strain.

The coupling between electrons and long wavelength phonons can be written in terms of the strain tensor. On symmetry grounds, we can define a scalar potential and a vector potential which change the effective Dirac equation which describes the electronic states [1,16–18]

$$V(\vec{\mathbf{r}}) = g_0[u_{xx}(\vec{\mathbf{r}}) + u_{yy}(\vec{\mathbf{r}})],$$
$$\vec{\mathbf{A}}(\vec{\mathbf{r}}) = \frac{\beta}{a}\left\{\frac{1}{2}[u_{xx}(\vec{\mathbf{r}}) - u_{yy}(\vec{\mathbf{r}})], -u_{xy}(\vec{\mathbf{r}})\right\}, \quad (4)$$

where $g_0 \approx 20$–30 eV is the bare deformation potential [16], $a \approx 1.4$ Å is the distance between nearest carbon atoms, $\beta = -\partial \log(t)/\partial \log(a) \approx 2$–$3$ [19], and $t \approx 3$ eV is the hopping between electrons in nearest carbon π orbitals.

Linearizing Eq. (1) and expressing the atomic displacements in terms of phonon creation and destruction operators, and using Eq. (4) and the Dirac Hamiltonian for graphene [1] we can write the full expressions for the coupling of charge carriers to longitudinal, transverse and FP, without and with preexisting strains.

Calculation of the resistivity.—We assume that the phonon energies are much less than the Fermi energy, so that the electron is scattered between states at the Fermi surface (see Fig. 1). The scattering rate has been obtained within the linearized Boltzmann equation, and the diagrams involved in this calculation are shown in Fig. 1 (for details see supplementary material [20]). Importantly, we have taken into account screening in the scalar potential, $g(K) = g_0/\varepsilon(K)$, given by the static dielectric function $\varepsilon(K) = 1 + e^2 N(k_F)/(2\epsilon_0 K)$, where $N(k_F) = (2k_F)/(\pi\hbar v_F)$ is the density of states, with v_F the Fermi velocity and k_F the Fermi momentum. At k_F the screened scalar potential $g \equiv g_0/\varepsilon(k_F) \approx g_0/8 \approx 3$ eV is in good agreement with *ab initio* calculations [21]. For the phonon dispersion we use Eq. (2) in the isotropic approximation, $\omega_q = \sqrt{\alpha^2 q^4 + \bar{u} v_L^2 q^2}$.

The relevant phonons which contribute to the resistivity are those of momenta $|\vec{\mathbf{q}}| \gtrsim 2k_F$. This scale allows us to define the Bloch-Grüneisen temperature, $k_B T_{\mathrm{BG}} = \hbar\omega_{2k_F}$. Neglecting first the effect of strain, we find

$$T_{\mathrm{BG}}^L = 57\sqrt{n}\ \mathrm{K} \qquad T_{\mathrm{BG}}^T = 38\sqrt{n}\ \mathrm{K} \qquad T_{\mathrm{BG}}^F = 0.1n\ \mathrm{K}, \quad (5)$$

respectively, for in-plane longitudinal (L) and transverse (T) and for FP (F), where the temperature is in Kelvin and the electron density n is expressed in 10^{12} cm^{-2}. Close to room T we are in the regime $T \gg T_{\mathrm{BG}}^{i=L,T,F}$ for all

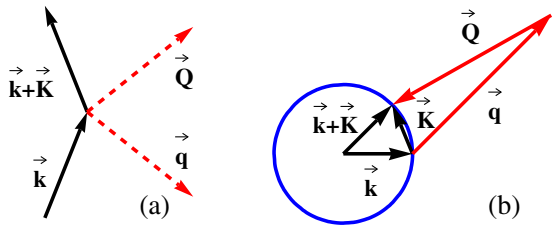

FIG. 1 (color online). (a) Two phonon diagram which describes electron scattering. (b) Kinematics of the process. The circle denotes the Fermi surface.

concentrations of interest. The corresponding temperature for FP in the presence of a uniaxial strain, $\bar{u}$ is $T_{\mathrm{BG}} = 28\sqrt{\bar{u}n}$ K. Our focus here is on the experimentally relevant high—T regime.

In systems with strain, the phonon dispersion relation, Eq. (2), shows a crossover between a regime dominated by strain to another where the strain becomes irrelevant, at $q^* \approx v_L\sqrt{\bar{u}}/\alpha$. The range of integration over the phonon momenta is limited by $\hbar\omega_q \lesssim k_B T$, and $k_F \lesssim q$. In addition the theory has a natural infrared cutoff with a characteristic momentum q_c below which the anharmonic effects become important [22]. Defining q_T as $\hbar\omega_{q_T} = k_B T$, the scattering rate shows three regimes in which (i) strain is irrelevant and $\max(q^*, q_c) \ll k_F$, (ii) strain is small and relevant phonons combine linear and quadratic spectrum for $\max(k_F, q_c) \lesssim q^* \lesssim q_T$, (iii) strain is high and determines the scattering rate for $q_T \ll q^*$. We finally obtain

$$\frac{1}{\tau_F} \approx \begin{cases} \frac{D^2(k_B T)^2}{64\pi\hbar^2\kappa^2 v_F k_F} \ln\left(\frac{k_B T}{\hbar\omega_c}\right) & \max(q^*, q_c) \ll k_F \ll q_T \\ \frac{D^2(k_B T)^2 k_F}{32\pi\hbar^2\rho\kappa v_F v_L^2 \bar{u}} & \max(k_F, q_c) \ll q^* \ll q_T, \\ \frac{6\zeta(3)D^2(k_B T)^4 k_F}{16\pi\hbar^4\rho^2 v_F v_L^6 \bar{u}^3} & k_F \ll q_T \ll q^* \end{cases} \quad (6)$$

where $D^2 = g^2/2 + (\beta\hbar v_F)^2/(4a^2)$, and the infrared cutoff $\hbar\omega_c$ is related to $\max(q^*, q_c)$. For comparison we give also the contribution from in-plane phonons,

$$\frac{1}{\tau_{L,T}} \approx \left[\frac{g^2}{v_L^2} + \frac{\beta^2\hbar^2 v_F^2}{4a^2}\left(\frac{1}{v_L^2} + \frac{1}{v_T^2}\right)\right]\frac{k_F k_B T}{2\rho\hbar^2 v_F}. \quad (7)$$

The T dependence of the scattering due to FP is more pronounced than that due to in-plane phonons, and it dominates at high enough T. In the limit of irrelevant strains, $\max(q^*, q_c) \ll k_F$, the crossover temperature is

$$\frac{\tau_{L,T}(T^*)}{\tau_F(T^*)} = 1 \Rightarrow T^*(\mathrm{K}) \approx 57 \times n(10^{12}\ \mathrm{cm}^{-2}). \quad (8)$$

When $T^* \lesssim T_{\mathrm{BG}}^{L,F}$ this crossover does not occur and scattering by FP dominates also at low temperatures. At finite strain $\max(k_F, q_c) \ll q^* \ll q_T$ we obtain

$$\frac{\tau_{L,T}(T^*)}{\tau_F(T^*)} = 1 \Rightarrow T^*(\mathrm{K}) \approx 10^6\bar{u}. \quad (9)$$

In the absence of strains, the crossover shown in Eq. (8) implies that the room T mobility is limited by FP for densities below 10^{13} cm^{-2}. Strains reduce significantly the effect of FP, so that, in the presence of strain, the mobility is determined by the scattering by in-plane phonons; see Eq. (9).

The contribution to the resistivity from the different phonon modes can be written, using the expressions for the scattering rate as

$$\varrho_i(n, T, \bar{u}) = \frac{2}{e^2 v_F^2 N(k_F)\tau_i(n, T, \bar{u})}, \quad (10)$$

where the index i label the phonon mode. Results for the resistivity in different regimes are shown in Fig. 2.

Experimental results.—We have fabricated two-terminal suspended devices following the procedures introduced in Refs. [5,6]. Typical changes in the resistance R as a function of the gate-induced concentration n are shown in Fig. 3(a). The as-fabricated devices exhibited $\mu \sim 1\ \mathrm{m}^2/\mathrm{V\,s}$ but, after their *in situ* annealing by electric current, μ could reach above $100\ \mathrm{m}^2/\mathrm{V\,s}$ at low T. To find μ, we have used the standard expression $R = R_0 + (l/w)(1/ne\mu)$, where R_0 describes the contact resistance plus the effect of neutral scatterers, and both R_0 and μ are assumed n independent [3,4]. Supplementary material provides examples of using this formula to analyze our experimental data [23]. Our devices had the length $l \approx 1$–$2\ \mu$m and the channel width w of 2–4 μm [see the inset in Fig. 3(b)]. At $T > 100$ K, the above expression describes well the functional form of the experimental curves, yielding a constant μ over the wide range of accessible n, if we allow R_0 to be different for electrons and holes [23]. This is expected because of an $n - p$ barrier that appears in the regime of electron doping due to our p-doping contacts [5,6]. At $T < 100$ K, the range of n over which the expression fits the data rapidly narrows. Below 20 K, we can use it only for $n < \pm 10^{10}\ \mathrm{cm}^{-2}$ because at higher n we enter into the ballistic regime (the mean free path, proportional to $\mu n^{1/2}$, becomes comparable to l). In the ballistic regime, graphene's conductivity σ is no longer proportional to n [5,6] and the use of μ as a transport parameter has no sense. To make sure that μ extracted over such a narrow range of n is also correct, we have crosschecked the found μ against the quantum mobilities inferred from the onset of Shubnikov–de Haas oscillations at low T [5,6,24] (also, see [23]). For all our devices with μ ranging from $\sim$1–100 $\mathrm{m}^2/\mathrm{V\,s}$, we find good agreement between transport and quantum mobilities at liquid-helium T, in agreement with earlier conclusions [6,24].

Figure 3(b) shows the T dependence of μ. It is well described by the quadratic dependence $1/\mu = 1/\mu(T \to 0) + \gamma T^2$. Surprisingly, we find the coefficient γ to vary by a factor of $\sim$2 for different devices [we measured eight suspended devices; data for three of them studied in detail are shown in Fig. 3(b)], which is unexpected for an intrinsic phonon contribution. Such variations are however expected if strain modifies electron-phonon scattering as discussed below. Note that μ falls down to 4–7 $\mathrm{m}^2/\mathrm{V\,s}$ at 200 K [see Fig. 3(b)] and the extrapolation to room T yields μ of only 2–3 $\mathrm{m}^2/\mathrm{V\,s}$, which is significantly lower than the values reported in Ref. [6] but in agreement with Ref. [5]. The disagreement between these two reports can also be reconciled by a strain suppressing the electron-phonon scattering.

Discussion.—The density independent $\mu \equiv 1/\varrho en$ indicates that experiments are in the nonstrained regime where FPs dominate. From Eq. (6) $1/\tau_F \sim T^2/k_F$, and using Eq. (10) $\varrho \sim T^2/n$. The coefficient γ is readily seen to be given by $\gamma \approx \frac{D^2 k_B^2}{64\pi e\hbar\kappa^2 v_F^2} \ln(\frac{k_B T}{\hbar\omega_c})$, where the infrared cutoff is the only free parameter [25]. Experiment gives $\gamma \approx 6.19 \times 10^{-6}\ \mathrm{V\,s/(mK)^2}$ for the sample with lower mobility and $\gamma \approx 3.32 \times 10^{-6}\ \mathrm{V\,s/(mK)^2}$ for the higher mobility one. Neglecting the logarithmic correction of order unity, the analytic expression gives $\gamma \approx 3 \times 10^{-6}\ \mathrm{V\,s/(mK)^2}$ without adjustable parameters.

The difference between samples may be understood as due to a different cutoff under the logarithm due to strain. In nonstrained samples there is a natural momentum cutoff $q_c \approx 0.1\ \text{Å}^{-1}$ below which the harmonic approximation breaks down [22]. Strain increases the validity range for the harmonic approximation, making q_c strain dependent, thus explaining different cutoff at different strain. A rough estimate of the expected strains is obtained by comparing $q_c \approx 0.1\ \text{Å}^{-1}$ with $q^* = v_L\sqrt{\bar{u}}/\alpha$, which gives $\bar{u} \sim 10^{-4} - 10^{-3}$, consistent with the strain reported in

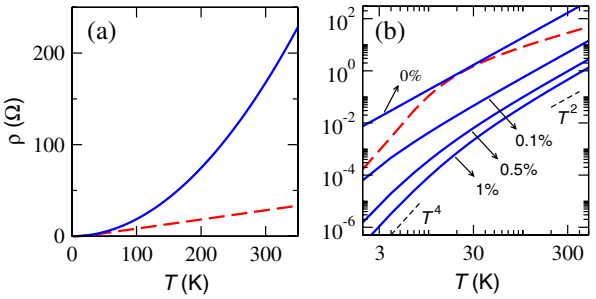

FIG. 2 (color online). (a) Contribution to the resistivity from flexural phonons (blue full line) and from in-plane phonons (red dashed line). (b) Resistivity for different strain. The in-plane contribution (broken red line) shows a crossover from a low to a high—T regime. In both cases, the electronic concentration is $n = 10^{12}\ \mathrm{cm}^{-2}$.

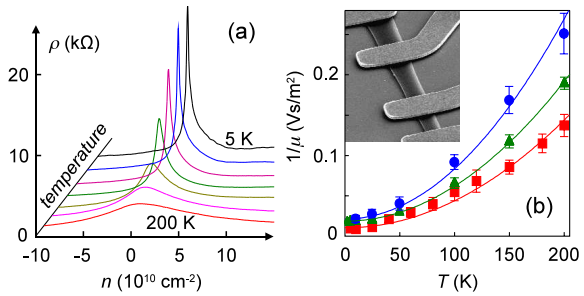

FIG. 3 (color online). (a) Electron transport in suspended graphene. Graphene resistivity $\varrho = R(w/l)$ as a function of gate-induced concentration n for $T = 5$, 10, 25, 50, 100, 150, and 200 K. (b) Examples of $\mu(T)$. The T range was limited by broadening of the peak beyond the accessible range of n. The inset shows a scanning electron micrograph of one of our suspended device. The darker nearly vertical stripe is graphene suspended below Au contacts. The scale is given by graphene width of about 1 μm for this particular device.

Ref. [26] for similar suspended devices. Strain induced by gate and T can be ruled out since we expect the present samples to be slacked. Indeed, graphene has a large negative thermal expansion coefficient ($\sim 10^{-5}/\mathrm{K}$) [13,27] and, because our measurements were done at T much lower than the T at which graphene was free to shrink along the substrate during microfabrication procedures ($\sim 150\,^{\circ}\mathrm{C}$), we can expect a slack of $>0.1\%$. Nevertheless, small strain can be present in the direction perpendicular to the slack due to, for example, the initial strain induced by the substrate and remaining unrelaxed under and near metal contacts. A complete theory would require the treatment of anharmonic effects, which is beyond the scope of the present work. For elevated temperatures ($T > 100$ K), the data in [7] show higher mobilities than those in Fig. 3. A fit to these data using Eq. (6) suggests that the sample was under significant strain.

Conclusions.—The experimental and theoretical results presented here suggest that FP are the main mechanism which limits the resistivity in suspended graphene samples, at temperatures above 10 K. Scattering by FP involves two modes, leading to a T^2 dependence at high temperatures, with mobility independent of carrier concentration. These results agree qualitatively with classical theory assuming elastic scattering by static thermally excited ripples [12]. Quantitatively, one of our main results is that in devices with little strain the mobility does not exceed values of the order of 1 $\mathrm{m^2V^{-1}\,s^{-1}}$ at room T, that is, FP restrict the electron mobility to values typical for exfoliated graphene on a substrate.

The dispersion of FP changes from quadratic to linear if the sample is under tension. As a result, the influence of FP on the transport properties is suppressed. The T dependence of resistivity remains quadratic but becomes much weaker. Moreover, in this regime phonon-induced resistivity is independent on n and the constant μ approximation breaks down. Importantly, applying rather weak strains may be enough to increase dramatically the mobility in freely suspended samples at room T.

A very recent theory work [28] has also addressed the role of FP on electron transport. Insofar as the two analysis partially overlap, the results are in agreement.

Useful discussions with Eros Mariani are gratefully acknowledged. We acknowledge financial support from MICINN (Spain) through grants FIS2008-00124 and CONSOLIDER CSD2007-00010, and from the Comunidad de Madrid, through NANOBIOMAG. M. I. K. acknowledges financial support from FOM (The Netherlands). The experimental part of the work was supported by EPSRC (UK), Körber Foundation, Office of Naval Research, Air Force Office of Scientific Research and the Royal Society.

[1] A. H. Castro Neto *et al.*, Rev. Mod. Phys. **81**, 109 (2009).
[2] A. K. Geim, Science **324**, 1530 (2009).
[3] S. V. Morozov *et al.*, Phys. Rev. Lett. **100**, 016602 (2008).
[4] J. H. Chen *et al.*, Nature Nanotech. **3**, 206 (2008).
[5] X. Du *et al.*, Nature Nanotech. **3**, 491 (2008).
[6] K. I. Bolotin *et al.*, Solid State Commun. **146**, 351 (2008).
[7] K. I. Bolotin *et al.*, Phys. Rev. Lett. **101**, 096802 (2008).
[8] E. H. Hwang and S. Das Sarma, Phys. Rev. B **77**, 115449 (2008).
[9] L. D. Landau and E. M. Lifschitz, *Theory of Elasticity* (Pergamon Press, Oxford, 1959).
[10] D. Nelson, in *Statistical Mechanics of Membranes and Surfaces*, edited by D. Nelson, T. Piran, and S. Weinberg (World Scientific, Singapore, 1989).
[11] E. Mariani and F. von Oppen, Phys. Rev. Lett. **100**, 076801 (2008).
[12] M. I. Katsnelson and A. K. Geim, Phil. Trans. R. Soc. A **366**, 195 (2008).
[13] K. V. Zakharchenko, M. I. Katsnelson, and A. Fasolino, Phys. Rev. Lett. **102**, 046808 (2009).
[14] C. Lee *et al.*, Science **321**, 385 (2008).
[15] K. N. Kudin, G. E. Scuseria, and B. I. Yakobson, Phys. Rev. B **64**, 235406 (2001).
[16] H. Suzuura and T. Ando, Phys. Rev. B **65**, 235412 (2002).
[17] J. L. Mañes, Phys. Rev. B **76**, 045430 (2007).
[18] M. A. H. Vozmediano, M. I. Katsnelson, and F. Guinea, Phys. Rep. **496**, 109 (2010).
[19] A. J. Heeger *et al.*, Rev. Mod. Phys. **60**, 781 (1988).
[20] See supplementary material at http://link.aps.org/supplemental/10.1103/PhysRevLett.105.266601.
[21] S.-M. Choi, S.-H. Jhi, and Y.-W. Son, Phys. Rev. B **81**, 081407 (2010).
[22] K. Zakharchenko *et al.*, Phys. Rev. B **82**, 125435 (2010).
[23] See supplementary material at http://link.aps.org/supplemental/10.1103/PhysRevLett.105.266601.
[24] M. Monteverde *et al.*, Phys. Rev. Lett. **104**, 126801 (2010).
[25] We fixed $g \approx 3$ eV and $\beta \approx 3$. These values are not only in agreement with theoretical predictions [19,21], they also perfectly reproduce the experimental data in Ref. [4] using Eqs. (7) and (10).
[26] C. Chen *et al.*, Nature Nanotech. **4**, 861 (2009).
[27] W. Bao *et al.*, Nature Nanotech. **4**, 562 (2009).
[28] E. Mariani and F. von Oppen, Phys. Rev. B **82**, 195403 (2010).